Crossover from charge density wave stabilized antiferromagnetism to superconductivity in $Nd_{1-x}La_xNiC_2$ compounds

Marta Roman,[1,*] Leszek Litzbarski,[1] Tomasz Klimczuk,[1] and Kamil K. Kolincio[1,2,†]

[1]*Faculty of Applied Physics and Mathematics, Gdansk University of Technology, Narutowicza 11/12, 80-233 Gdansk, Poland*
[2]*RIKEN Center for Emergent Matter Science, Wako, Saitama 351-0198, Japan*

The path from the charge density wave antiferromagnet NdNiC₂ to the noncentrosymmetric superconductor LaNiC₂ is studied by gradual replacement of Nd by La ions. The evolution of physical properties is explored by structural, magnetic, transport, magnetoresistance, and specific heat measurements. With the substitution of La for Nd, the Peierls temperature is gradually suppressed, which falls within the BCS mean-field relation for chemical pressure with a critical concentration of $x_c = 0.38$. As long as the charge density wave (CDW) is maintained, the antiferromagnetic (AFM) ground state remains robust against doping and, despite a Néel temperature reduction, shows a rapid and sharp magnetic transition. Once the CDW is completely suppressed, intermediate compounds of the $Nd_{1-x}La_xNiC_2$ series reveal symptoms of a gradual softening of the features associated with the AFM transition and an increase of the spin disorder. Immediately after the antiferromagnetic transition is depressed to zero temperature, the further incorporation of La ions results in the emergence of superconductivity. This crossover in $Nd_{1-x}La_xNiC_2$ is discussed in terms of the possible quantum critical point.

I. INTRODUCTION

The family of ternary rare-earth dicarbides RNiC₂ ($R = $ rare-earth metal) crystallizing in the noncentrosymmetric orthorhombic CeNiC₂-type crystal structure ($Amm2$) [1] has recently been extensively studied due to the variety of ground states which it offers. This family is known to exhibit, depending on the rare-earth atom, the charge density wave (CDW) at Peierls temperatures T_{CDW} ranging from 89 K for PrNiC₂ [2] to around 450 K for LuNiC₂ [3,4], superconductivity (SC), and ferromagnetism (FM) or antiferromagnetism (AFM) at low temperatures. So far the CDW state, which in RNiC₂ compounds is associated with the Ni atom chains constituting a quasi-low-dimensional electronic structure, has been found in most RNiC₂ members ($R = $ Pr–Lu) [3,5–10]. Recent studies revealed the linear scaling of the Peierls temperature with the unit-cell volume for $R = $ Sm–Lu [3]. The magnetism in RNiC₂, however, originates entirely from the rare-earth sublattice through the Ruderman-Kittel-Kasuya-Yosida (RKKY) interaction between local magnetic moments mediated by conducting electrons associated with the Ni atoms carrying no magnetic moment themselves [11,12]. With the exception of $R = $ (Y, La, Pr, Sm, Lu), all the RNiC₂ undergo an antiferromagnetic transition with Néel temperatures $T_N < 25$ K [12–20]. Only a weak magnetic anomaly was observed for PrNiC₂ [14,21], while SmNiC₂ [14] and LaNiC₂ [16,22–25] exhibit ferromagnetic and superconducting ground states, respectively. YNiC₂ and LuNiC₂ remain paramagnets above $T = 1.9$ K [4,12].

The vast diversity of physical properties offered by the RNiC₂ family makes them a promising platform to explore interrelationships between different types of ordering, especially between CDW, magnetism, and superconductivity. The recently explored interplay between CDW and magnetism has been found to exhibit a bilateral character. On the one hand, the antiferromagnetic state has been suggested to be created, or at least substantially reinforced, by the preexisting charge density wave state [26,27]. On the other hand, the same AFM state (NdNiC₂ and GdNiC₂) partially suppresses the CDW [2,21,28,29], although it allows the coexistence of both entities. Moreover, a completely destructive influence of ferromagnetism on the CDW was observed in SmNiC₂ [28,30–32]. In contrast, in PrNiC₂ the magnetic anomaly has been found to have a constructive impact on the nesting properties [2,21]. In such a group of materials, an even more fertile field allowing the exploration of these interactions opens up when two competing magnetic or electronic ground states tend towards zero temperature and the quantum fluctuations corresponding to them collide at a quantum critical point (QCP) [33–38]. A quantum critical point could be revealed and thus explored by tuning the ground state via nonthermal parameters such as pressure, composition, and magnetic field. The effect of pressure can be studied equivalently by applying external force or via chemical alloying, causing a change in the lattice parameters (increase or decrease, depending on the difference in atom size). The emergence of a ferromagnetic quantum criticality was previously suggested in SmNiC₂ studied under pressure [39], SmNiC₂₋ₓBₓ [40], and the $Sm_{1-x}La_xNiC_2$ solid solution [41,42]. So far, the antiferromagnetic QCPs in this family have been revealed under hydrostatic pressure in LaNiC₂ [25] and CeNiC₂ [43]. Alas, no signatures of quantum criticality have been observed in their solid solutions [44,45].

*marta.roman@pg.edu.pl
†kamkolin@pg.edu.pl

$LaNiC_2$ is an unconventional superconductor below $T_{SC} = 3$ K with magnetic-fluctuation-assisted Cooper pair creation [25]. The proximity of the AFM state seen in $NdNiC_2$ at $T_N = 17$ K (preceded also by a Peierls transition at $T_{CDW} = 121$ K) and this type of superconductivity in the phase diagram of $RNiC_2$ motivated us to use chemical alloying to explore the path between $NdNiC_2$ and $LaNiC_2$ from the vantage point of the evolution of the underlying ground states and the possible quantum criticality at AFM-SC crossover. In this paper, by means of structural, transport, magnetic, and heat capacity measurements we investigate the influence of La doping of $NdNiC_2$ on the charge density wave, antiferromagnetism, and superconductivity. A comprehensive T-x phase diagram showing a putative AFM QCP near $x^* = 0.88$ for the $Nd_{1-x}La_xNiC_2$ ($0 \leqslant x \leqslant 1$) series is constructed.

II. EXPERIMENT

The synthesis of the polycrystalline $Nd_{1-x}La_xNiC_2$ ($0 \leqslant x \leqslant 1$) series was performed via arc melting under a zirconium-gettered ultrapure argon atmosphere followed by further annealing at $900\,°C$ for 12 days. The purity of the elements used was 99.9% for Ni, 99.999% for C, 99.9% for Nd, and 99.99% for La; due to the high volatility of the lanthanides and carbon, 2% of Nd and La and 3% of C excess were added in order to compensate for the loss during arc melting. The overall change in weight after the synthesis process was negligible ($\leqslant 1\%$) indicating that the elemental concentration was close to the actual alloying level. The details for the whole procedure with the synthesis of other solid solutions were previously described in [27].

The phase purity of the samples from the whole series was confirmed by powder x-ray diffraction (PXRD) on a PANalytical X'Pert Pro diffractometer with a Cu K_α source. The lattice parameters were determined from a Le Bail profile refinement of the diffraction patterns by using FULLPROF [46] software.

The transport properties, magnetic susceptibility, and heat capacity were measured with a Quantum Design physical properties measurement system allowing the application of a magnetic field up to 9 T in the temperature range from 1.9 to 300 K. Magnetization measurements were performed using the ac and dc magnetometry system option. The ac magnetization for superconducting samples was measured with a dc field of 5 Oe and 1-kHz excitations with a 3-Oe amplitude. The specific heat measurements were performed using a standard relaxation method. The electrical resistivity was measured with a regular four-probe technique with thin ($\phi = 37\,\mu m$) Pt wires playing the role of electric contacts, which were spark welded to the polished surfaces of thin samples. The magnetoresistance was measured with magnetic field applied perpendicularly to the current direction.

III. RESULTS AND DISCUSSION

Diffraction patterns of the powdered samples from the $Nd_{1-x}La_xNiC_2$ ($0 \leqslant x \leqslant 1$) series were collected at room temperature and are depicted in Fig. 1. All observed reflections are successfully indexed in the orthorhombic $CeNiC_2$-type structure with space group $Amm2$, and no secondary phase was detected within the whole series. With increasing La content x in $Nd_{1-x}La_xNiC_2$ solid solutions, one can observe the shift of the Bragg reflection lines towards lower values of 2Θ, which is consistent with replacing Nd^{3+} ions with La^{3+} with a larger ionic radius [the shift of the main (111) reflection is shown in Fig. 1(b)]. The lattice parameters determined from the Le Bail fit for the whole $Nd_{1-x}La_xNiC_2$ series and for parent compounds $NdNiC_2$ and $LaNiC_2$ are in good agreement with previous reports [27,41]. As depicted in Fig. 1(c), the unit-cell parameters a, b, and c follow a linear relationship with the La doping rate x, and hence, Vegard's law is obeyed. The largest relative change is observed for the a parameter and reaches 4.5%, while the b change is barely noticeable (0.5%), which is associated with the rigid bond between carbon dimers arranged along the b axis [see the crystal structure picture in Fig. 1(c)].

The temperature dependence of the dc molar magnetic susceptibility χ_M for the whole $Nd_{1-x}La_xNiC_2$ series was measured in the temperature range 1.9–300 K with $\mu_0H = 1$ T applied magnetic field. Results for representative samples with $x \leqslant 0.9$ are presented in Fig. 2(a), whereas Fig. 2(b) depicts the reciprocal molar susceptibility as a function of temperature. At high temperatures all $Nd_{1-x}La_xNiC_2$ compounds show paramagnetic behavior. Upon cooling, at low temperatures one can observe a sharp maximum associated with an antiferromagnetic transition (for x ranging from $x = 0$ to $x = 0.5$). The Néel temperature, initially $T_N = 17$ K for $NdNiC_2$ ($x = 0$; in agreement with Ref. [27]), decreases with the rise in La concentration x and for $x = 0.5$ reaches $T_N = 9.5$ K. Starting from $x \geqslant 0.6$ the shape of the anomaly begins to broaden, and finally, for $x \geqslant 0.7$ the transition is no longer observed in the dc mode at an applied field of $\mu_0H = 1$ T. To distinguish between these two types of magnetic crossover, the Néel temperature is marked as T_N for the x range with a sharp character of transition and T_N^* for the region where the accompanying features are more blurred. T_N and T_N^* were estimated as the maximum of the temperature derivative of the real part of the magnetic susceptibility multiplied by the temperature $\frac{d(\chi_M'T)}{dT}$ (not shown here). To depict the contrast between these behaviors Fig. 2(a) (inset) shows the plots for $\chi_M(T)$ for $x = 0.2$ and $x = 0.6$, representative of sharp and blurred transition regions, respectively. The difference between them is likely associated with a weakening of the AFM interactions and an increase of spin disorder. This behavior differs from the results obtained for $Sm_{1-x}La_xNiC_2$ [41] and $SmNiC_{2-x}B_x$ [40], where weak doping initially causes a slight increase of Curie temperature T_C, followed by more abrupt suppression of FM for higher doping rates.

In $Nd_{1-x}La_xNiC_2$, above the AFM transition temperature, all $(\chi_M - \chi_0)^{-1}$ plots show an approximate linear dependence with T, indicating the relevance of the Curie-Weiss law expressed by the following equation:

$$\chi(T) = \frac{C}{T - \theta_{CW}} + \chi_0, \tag{1}$$

where C is the Curie constant, θ_{CW} is the Curie-Weiss temperature, and χ_0 is the temperature-independent magnetic susceptibility (in this case coming from both the sample and the sample holder). The Curie constant is related to the effective
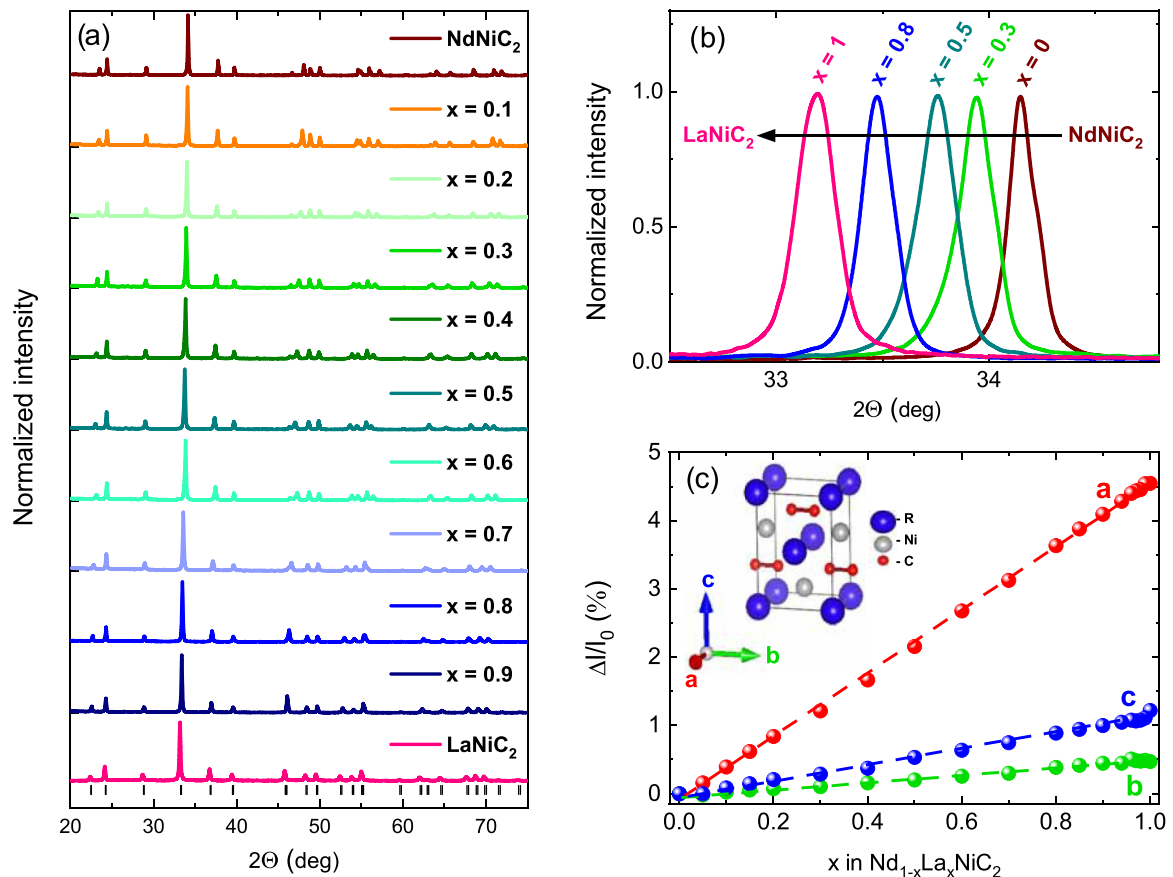
FIG. 1. (a) Normalized PXRD patterns for selected samples from the $Nd_{1-x}La_xNiC_2$ series. Bragg peak positions for $LaNiC_2$ are marked with vertical ticks. (b) Shift of the main (111) reflection with the change of x. (c) Relative change of the lattice parameters a, b, and c as a function of x.

magnetic moment μ_{eff} as

$$\mu_{\text{eff}} = \sqrt{\frac{3Ck_B}{\mu_B^2 N_A}}, \qquad (2)$$

where k_B is Boltzmann's constant, N_A is Avogadro's number, and μ_B is the Bohr magneton. The fit with Eq. (1) allowed the determination of the Curie-Weiss temperature and Curie constant, which were used to calculate the effective magnetic moment μ_{eff} [an exemplary fit in the temperature range 50–300 K to the data for $NdNiC_2$ is shown with a solid yellow line in Figs. 2(a) and 2(b)]. The Curie-Weiss temperature θ_{CW} and the effective magnetic moment μ_{eff} are presented in Figs. 2(c) and 2(d), respectively.

Upon the consequent increase of the La content in the $Nd_{1-x}La_xNiC_2$ solid solution, θ_{CW} starts to decrease its absolute value from $|\theta_{CW}| = 22.9$ K for $NdNiC_2$ [27], reaching an almost zero value for $x = 0.4$, which indicates a weakening of the AFM interactions between spins. This seems to be consistent with the decreasing concentration of magnetic Nd ions. For $x = 0.1$ one can notice the deviation from the general trend for θ_{CW}; however, the origin of this anomaly is not clear. By further replacing Nd by La ions one should expect a continuous weakening of the magnetic interactions, while the

Curie-Weiss temperature unexpectedly turns to more negative values up to $\theta_{CW} = -29.6$ K for $Nd_{0.1}La_{0.9}NiC_2$. For $x > 0.9$ the absolute value of the Curie-Weiss temperature begins to diminish in a quasilinear manner which coincides with the appearance of the superconducting state in compounds with a high La content range ($x \geqslant 0.96$). The gradual dilution of the Nd ions network with nonmagnetic La alone is not sufficient to explain either the Curie-Weiss temperature approaching zero for $x = 0.4$, where the magnetic order still persists, or the sudden return of θ_{CW} to more negative values as the La content is further increased ($0.4 < x < 0.9$). The presence of such an extremum points to an increase in the role of magnetic fluctuations or a more complex evolution of interactions between local magnetic moments.

The effective magnetic moment μ_{eff} varies with x in an approximately linear manner up to $x = 0.9$ [see Fig. 2(d)]. The value of μ_{eff} decreases from $4.1\mu_B$ [27] for $NdNiC_2$ with increasing La concentration x in $Nd_{1-x}La_xNiC_2$, which is consistent with the f electron number reduction caused by La substitution in place of Nd atoms. For $x > 0.9$ (marked by an arrow) μ_{eff} ceases to change linearly and drops abruptly towards a zero value for nonmagnetic $LaNiC_2$. This rapid fall of μ_{eff} is concomitant with the return of θ_{CW} towards zero.
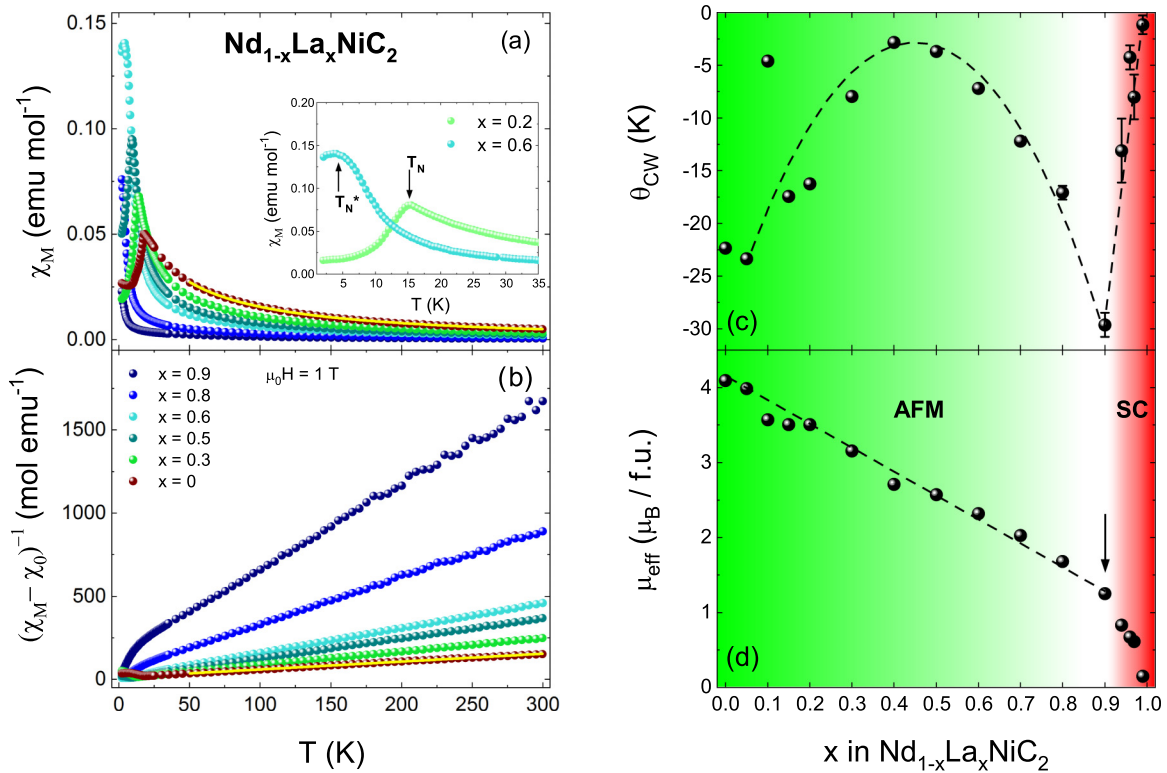
FIG. 2. Temperature dependence (a) of the molar magnetic susceptibility $\chi_M(T)$ and (b) of the reciprocal molar magnetic susceptibility $(\chi_M - \chi_0)^{-1}(T)$. Change of (c) the Curie-Weiss temperature θ_{CW} and (d) effective magnetic moment μ_{eff} with respect to composition x for the Nd$_{1-x}$La$_x$NiC$_2$ solid solution. The inset in (a) shows an expanded view of the low-temperature region for selected $x = 0.2$ and $x = 0.6$ compounds. Arrows indicate the transition temperatures T_N and T_N^*. Yellow solid lines in (a) and (b) represent the Curie-Weiss fit for NdNiC$_2$ (see text for details). Dashed lines in (c) and (d) are guides to the eyes, while the black arrow indicates the breakdown of linearity in $\mu_{\text{eff}}(x)$.

Superconductivity appears beyond the point at which the AFM is completely suppressed. The superconducting transition is revealed by the temperature dependence of the real part of the ac molar magnetization $M'(T)$, as depicted in Fig. 3(a). A sharp diamagnetic drop in the magnetization is observed for La-rich compounds, and the critical temperature increases with x from $T_{SC} = 1.98$ K for Nd$_{0.04}$La$_{0.96}$NiC$_2$ to $T_{SC} = 3$ K for LaNiC$_2$. Note that superconductivity persists only for small amounts of magnetic Nd dopant, which act as strong Cooper pair breaking centers.

In order to confirm the volume character of the superconducting transition, specific heat capacity measurements were performed, and $\frac{C_p}{T}(T^2)$ is presented in Fig. 3(b). For $x = 1$ a sharp superconducting transition is visible at $T_{SC} = 3$ K, and as Nd ions are introduced into LaNiC$_2$, the critical temperature decreases with simultaneous enhancement of a λ-shaped specific heat jump at the transition. Finally, for $x \leqslant 0.97$, although $\frac{C_p}{T}$ abruptly increases at low temperature, no maximum is observed above 1.9 K. This feature is *a priori* unexpected since one rather expects the weakening of the superconducting transition as T_{sc} is decreased and thus suggests the occurrence of an additional mechanism contributing to low-temperature specific heat. The experimental data points of the normal state were fitted using the formula

$$\frac{C_p}{T} = \gamma + \beta T^2, \tag{3}$$

where the first and second terms on the right side represent the electronic and lattice contributions to the specific heat, respectively. It is worth noting that the curves for $0.97 \leqslant x \leqslant 0.99$ present a similar slope and coincide with each other above $T \simeq 7.5$ K, indicating a barely noticeable change in thermodynamic parameters above the superconducting transition. The fit for $x = 0.99$ [black dashed line in Fig. 3(b)] provides values of the Sommerfeld coefficient $\gamma = 6.8(1)$ mJ mol^{-1} K^{-2} and $\beta = 0.102$ mJ mol^{-1} K^{-4}. The Debye temperature θ_D was estimated using a simple Debye model for the lattice contribution:

$$\theta_D = \left(\frac{12\pi^4}{5\beta} nR \right)^{\frac{1}{3}}, \tag{4}$$

where $R = 8.314$ mol^{-1} K^{-1} and n is the number of atoms per formula unit (here $n = 4$). The calculated θ_D shows a relatively high value of 423 K due to the presence of light carbon atoms. The obtained Sommerfeld coefficient and the Debye temperature are close to the values determined for LaNiC$_2$ (fit not shown), which are $\gamma = 6.6(0)$ mJ mol^{-1} K^{-2} and $\theta_D = 427$ K, respectively, also in agreement with previous reports [41].

The results of electronic transport measurements for the whole Nd$_{1-x}$La$_x$NiC$_2$ ($0 \leqslant x \leqslant 1$) series are presented in Fig. 4(a), where resistivity values are normalized to those at 300 K for comparison. Figures 4(b) and 4(c) delineate the resistivity curves $\rho/\rho_{20K}(T)$ for compounds showing AFM
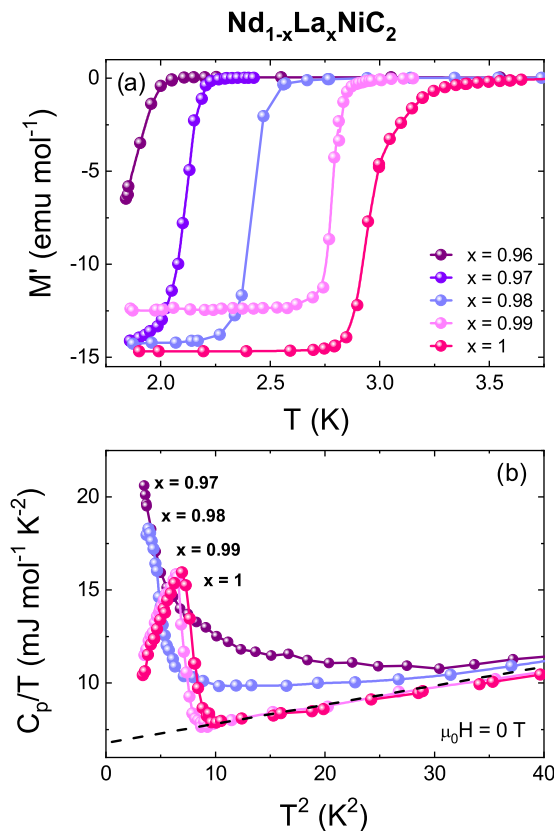
FIG. 3. (a) The real part of the molar magnetization $M'(T)$ and (b) heat capacity over temperature $C_p/T(T^2)$ for the superconducting samples ($x \geqslant 0.96$) from the $Nd_{1-x}La_xNiC_2$ series. A black dashed line represents a fit to $C_p/T = \gamma + \beta T^2$ in the normal state of the low-temperature region for the $x = 0.99$ sample.

and $\rho/\rho_{4K}(T)$ for samples exhibiting superconductivity, respectively.

The character of the resistivity evolves with x. At high temperatures, all compounds show typical metallic character with $\frac{d\rho}{dt} < 0$. For $x < 0.4$, the CDW metal-metal transition is observed at a Peierls temperature with a maximum value of $T_{CDW} = 121$ for $NdNiC_2$ that gradually decreases as Nd ions are replaced by La. The magnitude of the resistivity maximum accompanying the CDW transition decreases together with the Peierls temperature. In $Nd_{0.7}La_{0.3}NiC_2$ this anomaly is visible only as a weak inflection of the resistivity curve at $T_{CDW} = 53.5$ K, while for higher doping rates ($x > 0.3$) the Peierls transition is no longer observed, and the metallic character of the conductivity is preserved down to T_N or T_{SC}. At the Néel temperature a rapid drop in resistivity is observed for compounds with $x \leqslant 0.3$, thus those exhibiting a CDW. For compounds with $0.4 \leqslant x \leqslant 0.8$, the resistivity starts growing as the temperature is decreased below T_N^*. For $x = 0.9$ a small increase of $\rho(T)$ is observed at low temperatures; however, the magnetic susceptibility measurements do not detect any signatures of magnetic transition above $T = 1.9$ K [see Fig. 4(b) for an expanded view of low-temperature resistivity curves]. For $x > 0.9$, where the antiferromagnetic ground state is suppressed, the low-temperature behavior of resistivity evolves again and once more shows a decrease, this time reaching the zero value due to the superconducting transition [see

Fig. 4(c)]. Such a sharp crossover is visible for compounds with La content $x \geqslant 0.96$ with critical temperatures ranging from $T_{SC} = 2$ K for $x = 0.96$ to $T_{SC} = 3.2$ K for $x = 1$, thus slightly higher than estimated from magnetic and heat capacity measurements. For $x \leqslant 0.97$, despite a pronounced increase of $\frac{C_p}{T}$ at the lowest temperatures, no clear maximum can be observed above 1.9 K.

The increase in the resistivity below the Néel temperature is in contrast to the behavior seen in the $Sm_{1-x}La_xNiC_2$ solid solution [41], where the drop in resistivity was observed at the Curie temperature even for the intermediate compounds where the charge density wave was already suppressed. Previously, for parent $NdNiC_2$ the decrease of the resistivity at the magnetic ordering temperature was attributed both to the partial suppression of the charge density wave, concomitant with the release of condensed carriers, and the reduction of the spin disorder together with the underlying scattering rate [2,21,28]. This is also true for $GdNiC_2$ [26,47,48] and their solid solution $Nd_{1-x}Gd_xNiC_2$ in the whole x range [27]. A stronger effect was observed in $SmNiC_2$, where the charge density wave was completely suppressed [28,30–32]. In $Nd_{1-x}La_xNiC_2$ the resistivity drop below T_N is observed only for $\leqslant 0.3$, where the emergence of the CDW was detected; it is then reasonable to assume that this effect is, at least partially, caused by the weakening or the destruction of the charge density wave. Nevertheless, one should not underestimate the role played by the resistivity component associated with the spin disorder scattering. The reduction in the resistivity at T_N has also been observed in isostructural $CeNiC_2$ [21], deprived of the Peierls transition, which reflects the impact of spin fluctuations on the resistivity in the vicinity of T_N. Although for low values of x both terms appear to be relevant for high Nd concentrations, in the absence of a CDW for $x \geqslant 0.4$, the spin disorder is expected to play a decisive role in determining the form of $\rho(T)$ below the Néel temperature. It is surprising, however, not to observe the resistivity decreasing upon entering the magnetically ordered state, which is expected to be concomitant with the reduction of spin disorder as in $CeNiC_2$. The adverse direction of the resistivity evolution below T_N suggests rather the enhancement of the spin fluctuations instead of their condensation to long-range antiferromagnetism. Next to the spin disorder, the increase of resistance in this temperature range can partially originate from the Kondo effect, with dispersed magnetic ions acting as scattering centers [49,50]. We do not, however, find a logarithmic dependence of ρ as $T \to 0$, which is a characteristic feature of Kondo scattering with magnetic impurities [51,52]. The growth of $\rho(T)$ below T_N observed in $Nd_{1-x}La_xNiC_2$ does not lead to a maximum as reported in antiferromagnets with dominant Kondo interactions [53,54]. In these systems, resistivity drops significantly below the magnetic ordering temperature due to the suppression of spin disorder scattering as in regular AFM metals. The absence of such a drop and the continuous increase of $\rho(T)$ as $T \to 0$ suggest that the spin disorder scattering is a dominant mechanism, despite the increase of the role played by Kondo coupling in the terms of magnetic properties. The alternative scenario, the superzone boundary effect due to the mismatch between magnetic and crystallographical Brillouin zones observed in some AFM
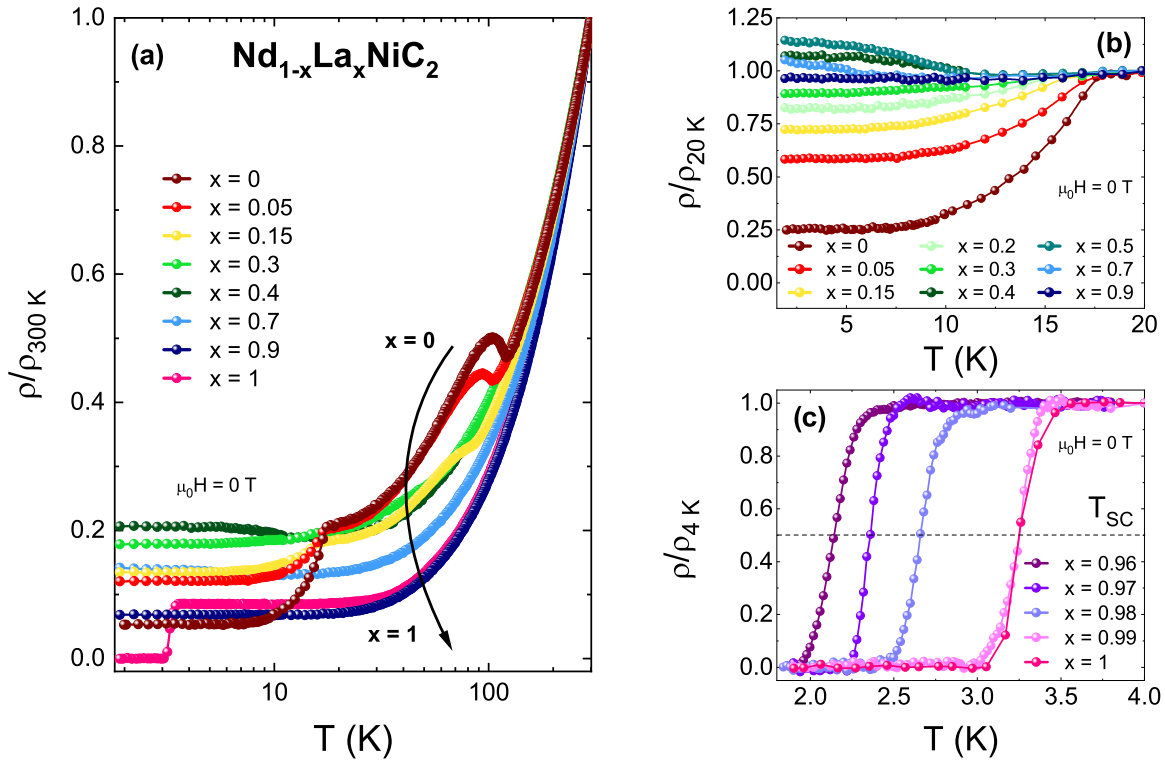
FIG. 4. (a) The thermal dependence of the normalized electrical resistivity for selected compounds from the $Nd_{1-x}La_xNiC_2$ solid solution in the temperature range from 1.9 to 300 K. For clarity, the scale for the horizontal axis is logarithmic. (b) and (c) Expanded views of the low-temperature region for $x \leqslant 0.9$ and $x > 0.9$, respectively.

systems [55,56], appears not to be relevant since the resistivity upturn is not seen for $Nd_{1-x}La_xNiC_2$ with high Nd concentrations and the Brillouin zone is not expected to significantly evolve between $NdNiC_2$ and $LaNiC_2$ since there are no drastic changes to the lattice parameters (see Fig. 1).

Complementary information on spin disorder can be obtained from magnetoresistance (MR) measurements. In Fig. 5 we compare the influence of magnetic field on the transport properties of selected members of the $Nd_{1-x}La_xNiC_2$ family, representative of the regions with distinct low-temperature resistivity behaviors. At temperatures far above the magnetic ordering, the magnetic field has a negligible impact on the resistivity. A stronger effect is visible as T is lowered. For $x = 0.1$ [Fig. 5(a)] the negative magnetoresistance term prevails both above and below Néel temperature. The character of the MR in this compound is reminiscent of the features seen in the parent $NdNiC_2$, where the suppression of the charge density wave plays a crucial role in the magnetoresistive effects [2,21,28]. By this analogy, it is reasonable to assume that the destruction of CDW is responsible for at least part of the MR in $Nd_{0.9}La_{0.1}NiC_2$. It is then not straightforward to isolate the spin scattering term from the whole magnetoresistance picture. For $x = 0.4$ [Fig. 5(b)], however, the CDW transition is no longer observed; thus, the spin fluctuations are expected to be the main driving force of the magnetoresistance [57–59]. The application of a magnetic field reduces the height of the resistivity hump observed below T_N, which can be attributed to a partial reorientation of the magnetic moments and a reduction of the magnetic entropy. The magnitude of this effect grows as the magnetic field is increased, and at $\mu_0H = 3$ T the

resistivity maximum is completely suppressed. Application of a stronger magnetic field continues to suppress the spin disorder and drives the resistivity even lower. Eventually, at high μ_0H, ρ ceases to decrease upon further increasing the magnetic field, presumably due to a final quench of the spin fluctuations by the field-induced ferromagnetic crossover. For $x = 0.9$ [Fig. 5(c)], showing no magnetic ordering down to 1.9 K, the application of a magnetic field suppresses the weak upturn of the zero-field-resistivity curve as $T \to 0$, unveiling a remarkably linear $\rho(T)$ dependence. A further increase of μ_0H beyond this point increases the value of resistivity, presumably due to the ordinary Lorentz mechanism, yet the linear $\rho(T)$ behavior is conserved at higher fields. The expanded view for the region with $\rho \sim T$ is highlighted in the inset of Fig. 5(c). For higher La concentrations, this term is less pronounced, as seen in Fig. 5(c). Finally, for $x \geqslant 0.97$ the linearity is no longer observed within the experimental resolution.

The transport results corroborate the magnetization measurements, showing a gradual softening of the features associated with the AFM transition as the Nd content in $Nd_{1-x}La_xNiC_2$ is decreased (thus x is increased). Both series of results reveal symptoms of disordered antiferromagnetic behavior for $x \geqslant 0.4$. Interestingly, this crossover coincides with the vanishing of the charge density wave state; compounds with a Peierls transition reveal a more ordered character than those in which the CDW is absent. It is plausible then to attribute this effect to the recently suggested stabilization of antiferromagnetism by the charge density wave via the Fermi surface nesting enhancement of the RKKY
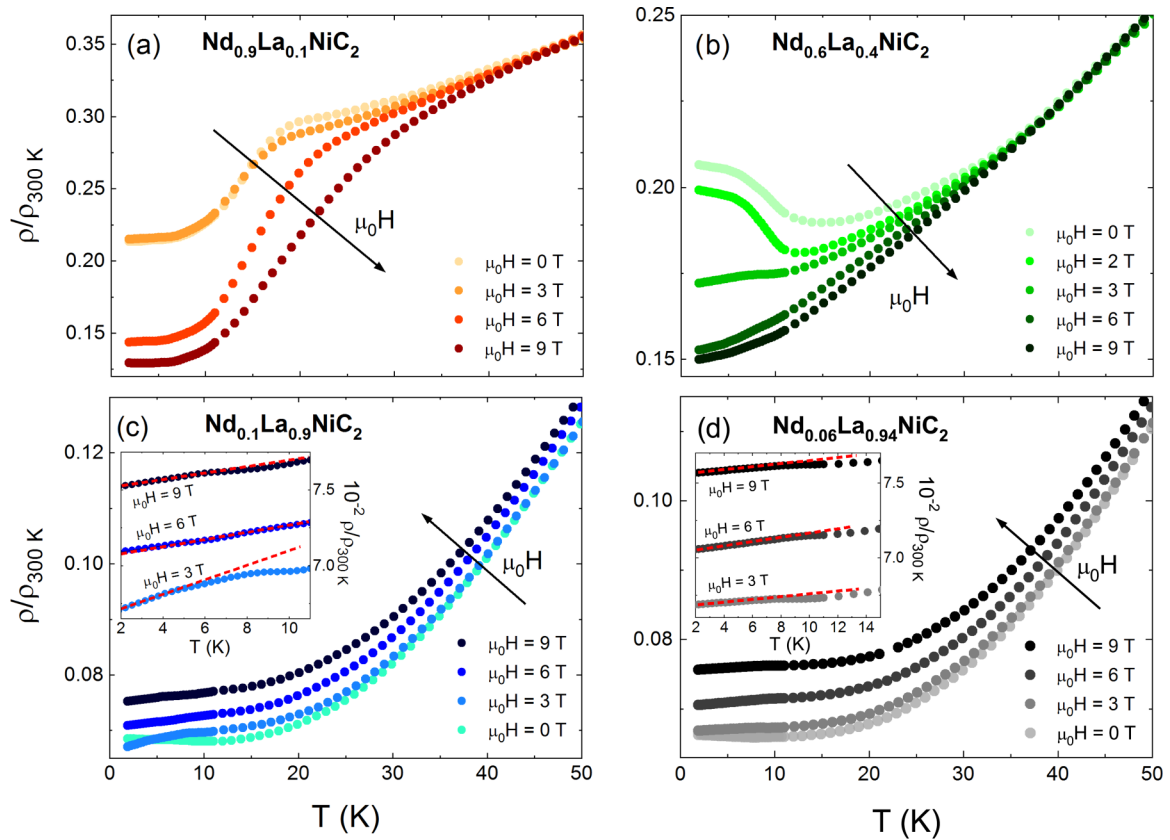
FIG. 5. The thermal variation of the normalized electrical resistivity measured at various magnetic fields for selected $Nd_{1-x}La_xNiC_2$ samples with (a) $x = 0.1$, (b) $x = 0.4$, (c) $x = 0.9$, and (d) $x = 0.94$. Insets in (c) and (d) show the expanded view of the region with linear $\rho(T)$. The dashed lines are a guide for the eye.

interaction between magnetic ions and the formation of a spin density wave in $GdNiC_2$, $NdNiC_2$, and their solid solutions [26,27,48]. When RKKY interaction is no longer enhanced by a charge density wave and its strength is weakened, the Doniach picture [60] predicts an increase of the role played by the Kondo interaction as the RKKY mechanism is weakened. This scenario can also explain the complex character of the $\theta_{CW}(x)$ curve. The initial decrease of $|\theta_{CW}|$ for $x < 0.4$ corresponds to the region where the CDW is gradually suppressed, which stands for the weakening of the RKKY mechanism, and as the charge density wave disappears, the paramagnetic Curie-Weiss temperature approaches zero. The further increase of La content beyond this point results in the inflection of $|\theta_{CW}|(x)$ in the region where the antiferromagnetic state is still present, although the thermal dependence of magnetic susceptibility and electrical resistance reveal signatures of magnetic fluctuations and a certain degree of disorder corresponding to them. Such an increase of $|\theta_{CW}|$ is expected to reflect the growth of the Kondo energy [61,62] that starts taking control over the magnetic ordering. The existence of magnetic fluctuations as well as the competition between Kondo and RKKY interactions can additionally lead to quantum critical behavior of magnetic ordering [62,63].

To summarize the results from both magnetic and transport measurements, they were used to construct the phase diagram for the $Nd_{1-x}La_xNiC_2$ ($0 \leqslant x \leqslant 1$) series, which is depicted in Fig. 6. Blue represents the region in which the CDW is observed with the Peierls temperature gradually suppressed

from $T_{CDW} = 121$ K for $NdNiC_2$ with increasing La concentration. $T_{CDW}(x)$ is successfully described by a mean-field power law function characterizing the influence of chemical pressure [40,64,65]:

$$T_{CDW} = T_{CDW}(0)\sqrt{1 - \frac{x}{x_c}}, \qquad (5)$$

where $T_{CDW}(0)$ is the temperature of the CDW transition for $x = 0$ and x_c is the La content corresponding to $T_{CDW} = 0$ K. Constraining the fit with constant $T_{CDW} = 121$ K for undoped $NdNiC_2$ gives the value of $x_c = 0.38$, slightly below the first point ($x = 0.4$) at which the CDW transition is no longer observed. The fit to Eq. (5) is shown in Fig. 6 as a blue line. The AFM region is represented in green; dark and light green points stand for T_N and T_N^*, respectively. The decrease of the Néel temperature is not as steep as in the case of T_{CDW}, and for $x = 0.9$ AFM is no longer observed above $T = 1.9$ K. A further increase of La concentration results in an almost immediate onset of superconductivity (represented by red in Fig. 6), which rises for $x \geqslant 0.96$, and critical temperature starts to increase with x. The inset of Fig. 6 presents an expanded view of the antiferromagnetic and superconducting regions. Curves describing the x dependence of the Néel and critical temperatures can be extrapolated to $T = 0$ K. Interestingly, both lines intersect at zero temperature near $x^* = 0.88$, suggesting the putative existence of the AFM quantum critical point in the $Nd_{1-x}La_xNiC_2$ series. Typically, the quantum criticality is accompanied by characteristic

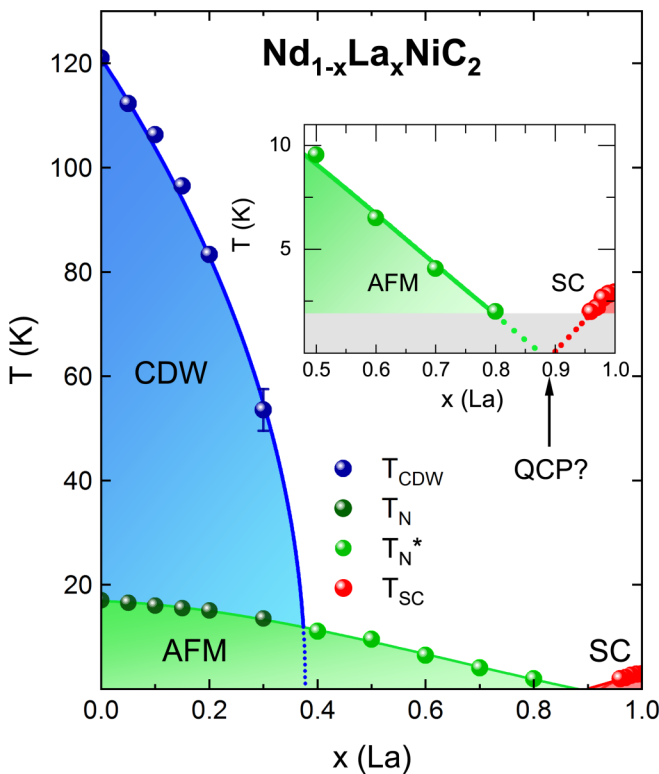FIG. 6. Phase diagram of temperature vs composition $(T - x)$ for the $Nd_{1-x}La_xNiC_2$ series. The CDW phase with Peierls temperature T_{CDW} is represented by gradient blue color. The AFM phase with T_N and T_N^* is represented by gradient green color, and SC with the T_{SC} phase is shown in red. The Néel temperature for the AFM crossovers with distinct characters is marked by dark green points for the region in which the transition is sharp (T_N) and by light green points where the AFM transition is blurred and accompanying anomalies are weakened (T_N^*). The blue line is the fit to $T_{CDW}(x)$ with Eq. (5). The inset shows an expanded view of the low-temperature region to highlight the collision of the AFM and SC regions at a possible quantum critical point marked by a black arrow.

features in electrical resistivity in the vicinity of a QCP [66,67]. This effect is expected to be pronounced by the softening of the temperature dependence of resistivity via a reduction of the exponent p in

$$\rho(T) = \rho_0 + AT^p, \qquad (6)$$

where ρ_0 is the residual resistivity and the second term stands for the resistivity component dependent on temperature with p, indicating the prevailing type of scattering: $p = 1$ is expected in quantum critical regime [68,69].

The linearity of $\rho(T)$ was reported in a wide concentration range near the ferromagnetic QCP in $SmNiC_{1-x}B_x$ [40] and $SmNiC_2$ under pressure [39]. The signatures of such an effect in $Nd_{1-x}La_xNiC_2$ are seen only in $\rho(T)$ curves measured in the presence of external magnetic field, for $0.6 < x < 0.97$, close to the presumed QCP at $x = 0.88$. A plausible scenario is that the linear, non-Fermi-liquid behavior buried beneath the low-temperature upturn in resistivity is uncovered by the magnetic field quenching the spin disorder scattering. It will, however, be mentioned that, typically, a critical region with a non-Fermi-liquid behavior is confined to a narrow vicinity

of a QCP [70,71], while the linearity in transport properties of $Nd_{1-x}La_xNiC_2$ is seen in an asymmetric zone, extended in the direction of low La concentrations. Although there are exceptions, such as a rather wide quantum critical region accompanying the transition from spiral to ferromagnetic phases in $ZnCr_2Se_4$ [72], in $Nd_{1-x}La_xNiC_2$ the linear $\rho(T)$ dependence near the AFM-SC crossover can also originate from other factors, such as the direct impact of spin scattering. Therefore, this effect cannot be treated as clear evidence of a QCP, but rather as a clue pointing towards its possible occurrence.

The possibility of quantum critical behavior even in the complete absence of resistivity softening was recently concluded based on the clear increase in $\frac{C_p}{T}$ as $T \to 0$ on the superconducting side of a presumed QCP in $Sm_{1-x}La_xNiC_2$ [41]. An analogous situation is observed in $Nd_{1-x}La_xNiC_2$, where the magnitude of the specific heat jump near the onset of superconductivity notably increases despite the critical temperature being gradually suppressed as La atoms are substituted with Nd. Since the SC is weakened, the enhancement of $\frac{C_p}{T}$ likely stems from fluctuations emerging at low temperature. On the one hand, their origin can be purely magnetic due to the vicinity of the AFM state. On the other hand, such a singular amplification of specific heat in the low-temperature limit when $x \to x^*$ is a typical feature of critical order parameter fluctuations in the vicinity of a QCP [73–76]. It is possible then to attribute the growth of low-temperature C_p, at least partially, to the latter term. To unambiguously clarify the nature of the AFM-to-SC crossover, the transport and specific heat measurements must be extended to He^3 temperatures. Alternative methods are nuclear magnetic resonance [77], neutron diffraction, and muon spectroscopy [42], allowing one to directly confirm (or deny) the quantum criticality near the point of contact of these two types of order parameters.

IV. CONCLUSIONS

The $Nd_{1-x}La_xNiC_2$ ($0 \leqslant x \leqslant 1$) solid solutions have been synthesized. By consequent replacement of Nd with La ions, the evolution from $NdNiC_2$ revealing both the CDW and AFM state to the noncentrosymmetric unconventional superconductor $LaNiC_2$ has been investigated. The structural changes caused by doping-induced chemical pressure manifested in the linear variation of structural parameters, in agreement with Vegard's law. The substitution of La in Nd positions results in an abrupt suppression of the charge density wave, and for La content higher than $x = 0.4$ this ordering is no longer observed. We have found that as long as the CDW state is preserved, the AFM ground state shows strong anomalies in magnetic susceptibility and transport properties. With the further increase of La concentration, for compounds where the CDW is completely suppressed, the features associated with AFM transition become smeared, which is accompanied by the signatures of spin disorder, leading to a resistivity increase below the temperature of the magnetic anomaly and negative magnetoresistance. Such a crossover suggests a strong role is played by the charge density wave in the stabilization of antiferromagnetism via formation of a spin density wave in the presence of strong local magnetic moments. The gradually suppressed magnetism is replaced by

superconductivity observed for La-rich compounds (for $x >$ 0.96), where the critical temperature quickly diminishes with a small amount of magnetic Nd ions. The results of magnetic and transport properties of the $Nd_{1-x}La_xNiC_2$ ($0 \leqslant x \leqslant 1$) series were summarized in a comprehensive T-x phase diagram. The extrapolation of curves following the variations of characteristic temperatures for antiferromagnetic order (T_N) and superconductivity (T_{sc}) suggests the putative existence of a critical point near $x^* = 0.88$ where these two entities subside to zero temperature. The characteristic features that can be seen as signatures of quantum criticality can be found in specific heat and transport properties.

[1] W. Jeitschko and M. H. Gerss, J. Less-Common Met. **116**, 147 (1986).

[2] N. Yamamoto, R. Kondo, H. Maeda, and Y. Nogami, J. Phys. Soc. Jpn. **82**, 123701 (2013).

[3] M. Roman, J. Strychalska-Nowak, T. Klimczuk, and K. K. Kolincio, Phys. Rev. B **97**, 041103(R) (2018).

[4] S. Steiner, H. Michor, O. Sologub, B. Hinterleitner, F. Höfenstock, M. Waas, E. Bauer, B. Stöger, V. Babizhetskyy, V. Levytskyy, and B. Kotur, Phys. Rev. B **97**, 205115 (2018).

[5] M. Murase, A. Tobo, H. Onodera, Y. Hirano, T. Hosaka, S. Shimomura, and N. Wakabayashi, J. Phys. Soc. Jpn. **73**, 2790 (2004).

[6] J. Laverock, T. D. Haynes, C. Utfeld, and S. B. Dugdale, Phys. Rev. B **80**, 125111 (2009).

[7] A. Wölfel, L. Li, S. Shimomura, H. Onodera, and S. van Smaalen, Phys. Rev. B **82**, 054120 (2010).

[8] T. Sato, S. Souma, K. Nakayama, T. Takahashi, S. Shimomura, and H. Onodera, J. Phys. Soc. Jpn. **79**, 044707 (2010).

[9] D. Ahmad, B. H. Min, G. I. Min, S.-I. Kimura, J. Seo, and Y. S. Kwon, Phys. Status Solidi B **252**, 2662 (2015).

[10] H. Michor, S. Steiner, A. Schumer, M. Hembara, V. Levytskyy, V. Babizhetskyy, and B. Kotur, J. Magn. Magn. Mater. **441**, 69 (2017).

[11] W. Schäfer, W. Kockelmann, G. Will, J. Yakinthos, and P. Kotsanidis, J. Alloys Compd. **250**, 565 (1997).

[12] P. Kotsanidis, J. Yakinthos, and E. Gamari-Seale, J. Less-Common Met. **152**, 287 (1989).

[13] H. Onodera, M. Ohashi, H. Amanai, S. Matsuo, H. Yamauchi, Y. Yamaguchi, S. Funahashi, and Y. Morii, J. Magn. Magn. Mater. **149**, 287 (1995).

[14] H. Onodera, Y. Koshikawa, M. Kosaka, M. Ohashi, H. Yamauchi, and Y. Yamaguchi, J. Magn. Magn. Mater. **182**, 161 (1998).

[15] A. Bhattacharyya, D. T. Adroja, A. M. Strydom, A. D. Hillier, J. W. Taylor, A. Thamizhavel, S. K. Dhar, W. A. Kockelmann, and B. D. Rainford, Phys. Rev. B **90**, 054405 (2014).

[16] V. K. Pecharsky, L. L. Miller, and K. A. Gschneidner, Phys. Rev. B **58**, 497 (1998).

[17] J. Yakinthos, P. Kotsanidis, W. Schäfer, and G. Will, J. Magn. Magn. Mater. **89**, 299 (1990).

[18] N. Hanasaki, K. Mikami, S. Torigoe, Y. Nogami, S. Shimomura, M. Kosaka, and H. Onodera, J. Phys.: Conf. Ser. **320**, 012072 (2011).

[19] N. Uchida, H. Onodera, M. Ohashi, Y. Yamaguchi, N. Sato, and S. Funahashi, J. Magn. Magn. Mater. **145**, L16 (1995).

[20] S. Matsuo, H. Onodera, M. Kosaka, H. Kobayashi, M. Ohashi, H. Yamauchi, and Y. Yamaguchi, J. Magn. Magn. Mater. **161**, 255 (1996).

[21] K. K. Kolincio, M. Roman, M. J. Winiarski, J. Strychalska-Nowak, and T. Klimczuk, Phys. Rev. B **95**, 235156 (2017).

[22] B. Wiendlocha, R. Szczśniak, A. P. Durajski, and M. Muras, Phys. Rev. B **94**, 134517 (2016).

[23] W. H. Lee, H. K. Zeng, Y. D. Yao, and Y. Y. Chen, Phys. C (Amsterdam, Neth.) **266**, 138 (1996).

[24] J. Quintanilla, A. D. Hillier, J. F. Annett, and R. Cywinski, Phys. Rev. B **82**, 174511 (2010).

[25] J. F. Landaeta, D. Subero, P. Machado, F. Honda, and I. Bonalde, Phys. Rev. B **96**, 174515 (2017).

[26] N. Hanasaki, S. Shimomura, K. Mikami, Y. Nogami, H. Nakao, and H. Onodera, Phys. Rev. B **95**, 085103 (2017).

[27] M. Roman, T. Klimczuk, and K. K. Kolincio, Phys. Rev. B **98**, 035136 (2018).

[28] H. Lei, K. Wang, and C. Petrovic, J. Phys.: Condens. Matter **29**, 075602 (2017).

[29] K. K. Kolincio, R. Daou, O. Pérez, L. Guérin, P. Fertey, and A. Pautrat, Phys. Rev. B **94**, 241118(R) (2016).

[30] S. Shimomura, C. Hayashi, G. Asaka, N. Wakabayashi, M. Mizumaki, and H. Onodera, Phys. Rev. Lett. **102**, 076404 (2009).

[31] N. Hanasaki, Y. Nogami, M. Kakinuma, S. Shimomura, M. Kosaka, and H. Onodera, Phys. Rev. B **85**, 092402 (2012).

[32] J. H. Kim, J.-S. Rhyee, and Y. S. Kwon, Phys. Rev. B **86**, 235101 (2012).

[33] A. Kopp and S. Chakravarty, Nat. Phys. **1**, 53 (2005).

[34] D. J. Scalapino, Rev. Mod. Phys. **84**, 1383 (2012).

[35] S. Friedemann, T. Westerkamp, M. Brando, N. Oeschler, S. Wirth, P. Gegenwart, C. Krellner, C. Geibel, and F. Steglich, Nat. Phys. **5**, 465 (2009).

[36] X. Wang, Y. Wang, Y. Schattner, E. Berg, and R. M. Fernandes, Phys. Rev. Lett. **120**, 247002 (2018).

[37] H. Jang, W.-S. Lee, H. Song, H. Nojiri, S. Matsuzawa, H. Yasumura, H. Huang, Y.-J. Liu, J. Porras, M. Minola, B. Keimer, J. Hastings, D. Zhu, T. P. Devereaux, Z.-X. Shen, C.-C. Kao, and J.-S. Lee, Phys. Rev. B **97**, 224513 (2018).

[38] Y. Wang, T. F. Rosenbaum, A. Palmer, Y. Ren, J.-W. Kim, D. Mandrus, and Y. Feng, Nat. Commun. **9**, 2953 (2018).

[39] B. Woo, S. Seo, E. Park, J. H. Kim, D. Jang, T. Park, H. Lee, F. Ronning, J. D. Thompson, V. A. Sidorov, and Y. S. Kwon, Phys. Rev. B **87**, 125121 (2013).

[40] F. Morales, L. F. Mendivil, and R. Escamilla, J. Phys.: Condens. Matter **26**, 455602 (2014).

[41] G. Prathiba, I. Kim, S. Shin, J. Strychalska, T. Klimczuk, and T. Park, Sci. Rep. **6**, 26530 (2016).

[42] W. Lee, S. Lee, K.-Y. Choi, K.-J. Lee, B.-J. Kim, B. J. Suh, S. Shin, and T. Park, Phys. Rev. B **96**, 224433 (2017).

[43] S. Katano, M. Ito, K. Shibata, J. Gouchi, Y. Uwatoko, K. Matsubayashi, H. Soeda, and H. Takahashi, Phys. Rev. B **99**, 100501(R) (2019).

[44] S. Katano, K. Shibata, K. Nakashima, H. Yoshimura, and Y. Matsubara, J. Phys. Soc. Jpn. **86**, 104704 (2017).

[45] S. Katano, K. Shibata, K. Nakashima, and Y. Matsubara, Phys. Rev. B **95**, 144502 (2017).

[46] J. Rodríguez-Carvajal, Phys. B (Amsterdam, Neth.) **192**, 55 (1993).

[47] S. Shimomura, C. Hayashi, N. Hanasaki, K. Ohnuma, Y. Kobayashi, H. Nakao, M. Mizumaki, and H. Onodera, Phys. Rev. B **93**, 165108 (2016).

[48] K. K. Kolincio, K. Górnicka, M. J. Winiarski, J. Strychalska-Nowak, and T. Klimczuk, Phys. Rev. B **94**, 195149 (2016).

[49] J. Kondo, Prog. Theor. Phys. **32**, 37 (1964).

[50] B. A. Jones, in *Handbook of Magnetism and Advanced Magnetic Materials* (John Wiley & Sons, Pennsylvania, 2007).

[51] A. Pautrat and W. Kobayashi, Phys. Rev. B **82**, 115113 (2010).

[52] H. Rotella, A. Pautrat, O. Copie, P. Boullay, A. David, B. Mercey, M. Morales, and W. Prellier, J. Phys.: Condens. Matter **27**, 435601 (2015).

[53] M. Nakashima, Y. Amako, K. Matsubayashi, Y. Uwatoko, M. Nada, K. Sugiyama, M. Hagiwara, Y. Haga, T. Takeuchi, A. Nakamura, H. Akamine, K. Tomori, T. Yara, Y. Ashitomi, M. Hedo, T. Nakama, and Y. Ōnuki, J. Phys. Soc. Jpn. **86**, 034708 (2017).

[54] A. Nakamura, T. Okazaki, M. Nakashima, Y. Amako, K. Matsubayashi, Y. Uwatoko, S. Kayama, T. Kagayama, K. Shimizu, T. Uejo, H. Akamine, M. Hedo, T. Nakama, Y. Ōnuki, and H. Shiba, J. Phys. Soc. Jpn. **84**, 053701 (2015).

[55] T. Klimczuk, P. Boulet, J.-C. Griveau, E. Colineau, E. Bauer, M. Falmbigl, P. Rogl, and F. Wastin, Philos. Mag. **95**, 649 (2015).

[56] R. J. Elliott and F. A. Wedgwood, Proc. Phys. Soc. **81**, 846 (1963).

[57] C. Mazumdar, A. K. Nigam, R. Nagarajan, L. C. Gupta, G. Chandra, B. D. Padalia, C. Godart, and R. Vijayaraghaven, J. Appl. Phys. **81**, 5781 (1997).

[58] H. Yamada and S. Takada, Prog. Theor. Phys. **48**, 1828 (1972).

[59] M. Akhavan and H. A. Blackstead, Phys. Rev. B **13**, 1209 (1976).

[60] S. Doniach, Phys. B+C (Amsterdam) **91**, 231 (1977).

[61] H. R. Krishna-murthy, K. G. Wilson, and J. W. Wilkins, Phys. Rev. Lett. **35**, 1101 (1975).

[62] Y. Lai, S. E. Bone, S. Minasian, M. G. Ferrier, J. Lezama-Pacheco, V. Mocko, A. S. Ditter, S. A. Kozimor, G. T. Seidler, W. L. Nelson, Y.-C. Chiu, K. Huang, W. Potter, D. Graf, T. E. Albrecht-Schmitt, and R. E. Baumbach, Phys. Rev. B **97**, 224406 (2018).

[63] G. Knebel, C. Eggert, D. Engelmann, R. Viana, A. Krimmel, M. Dressel, and A. Loidl, Phys. Rev. B **53**, 11586 (1996).

[64] R. Jaramillo, Y. Feng, J. C. Lang, Z. Islam, G. Srajer, P. B. Littlewood, D. B. McWhan, and T. F. Rosenbaum, Nature (London) **459**, 405 (2009).

[65] M. Monteverde, J. Lorenzana, P. Monceau, and M. Núñez-Regueiro, Phys. Rev. B **88**, 180504(R) (2013).

[66] S. Sachdev and B. Keimer, Phys. Today **64(2)**, 29 (2011).

[67] P. Coleman and A. J. Schofield, Nature (London) **433**, 226 (2005).

[68] M. Gooch, B. Lv, B. Lorenz, A. M. Guloy, and C.-W. Chu, Phys. Rev. B **79**, 104504 (2009).

[69] G. R. Stewart, Rev. Mod. Phys. **73**, 797 (2001).

[70] A. Narayan, A. Cano, A. V. Balatsky, and N. A. Spaldin, Nat. Mater. **18**, 223 (2019).

[71] S. A. Grigera, R. S. Perry, A. J. Schofield, M. Chiao, S. R. Julian, G. G. Lonzarich, S. I. Ikeda, Y. Maeno, A. J. Millis, and A. P. Mackenzie, Science **294**, 329 (2001).

[72] C. C. Gu, Z. Y. Zhao, X. L. Chen, M. Lee, E. S. Choi, Y. Y. Han, L. S. Ling, L. Pi, Y. H. Zhang, G. Chen, Z. R. Yang, H. D. Zhou, and X. F. Sun, Phys. Rev. Lett. **120**, 147204 (2018).

[73] L. Zhu, M. Garst, A. Rosch, and Q. Si, Phys. Rev. Lett. **91**, 066404 (2003).

[74] A. Steppke, R. Küchler, S. Lausberg, E. Lengyel, L. Steinke, R. Borth, T. Lühmann, C. Krellner, M. Nicklas, C. Geibel, F. Steglich, and M. Brando, Science **339**, 933 (2013).

[75] T. Westerkamp, M. Deppe, R. Küchler, M. Brando, C. Geibel, P. Gegenwart, A. P. Pikul, and F. Steglich, Phys. Rev. Lett. **102**, 206404 (2009).

[76] C. J. Sheppard, A. R. E. Prinsloo, H. L. Alberts, and A. M. Strydom, J. Appl. Phys. **109**, 07E104 (2011).

[77] A. W. Kinross, M. Fu, T. J. Munsie, H. A. Dabkowska, G. M. Luke, S. Sachdev, and T. Imai, Phys. Rev. X **4**, 031008 (2014).